Atmos. Meas. Tech. Discuss., https://doi.org/10.5194/amt-2017-432
Manuscript under review for journal Atmos. Meas. Tech.
Discussion started: 11 January 2018

Atmospheric Measurement Techniques Discussions
Open Access

The instrument constant of sky radiometer (POM-02), Part I: Calibration constant

Akihiro Uchiyama[1], Tsuneo Matsunaga[1] , Akihiro Yamazaki[2]

[1] Center for Global Environmental Research, National Institute for Environmental Studies, Tsukuba, Ibaraki, 305-8506, Japan

[2] Meteorological Research Institute, Japan Meteorological Agency, Tsukuba, Ibaraki, 305-0052, Japan

Corresponding to: Uchiyama Akihiro (uchiyama.akihiro@nies.go.jp)

Abstract

Ground-based networks have been developed to determine the spatiotemporal distribution of aerosols using radiometers. In this study, the accuracy of the calibration constant (V_0) for the sky radiometer (POM-02) which is used by SKYNET was investigated. The temperature dependence of the sensor output was also investigated, and the dependence in the 340, 380, and 2200 nm channels was found to be larger than for other channels, and varied with the instrument. In the summer, the sensor output had to be corrected by a factor of 1.5 to 2% in the 340 and 380 nm channels and by 4% in the 2200 nm channel in the measurements at Tsukuba. In the other channels, the correction factors were less than 0.5%. The accuracy of V_0 from the normal Langley method is between 0.2 and 1.3%, except in the 940 nm channel. The effect of gas absorption was less than 1% in the 1225, 1627, and 2200 nm channels. The degradation of V_0 for shorter wavelengths was larger than that for longer wavelengths. The accuracy of V_0 estimated from the side-by-side measurements was

Atmos. Meas. Tech. Discuss., https://doi.org/10.5194/amt-2017-432
Manuscript under review for journal Atmos. Meas. Tech.
Discussion started: 11 January 2018

0.1 to 0.5%. The V_0 determined by the improved Langley (IML) method had a seasonal variation of 1 to 3%. The RMS error from the IML method was about 0.6 to 2.5%, and in some cases, the maximum difference reached 5%. The trend in V_0 after removing the seasonal variation was almost the same as for the normal Langley method. The calibration method for water vapor in the 940 nm channel was developed using an empirical formula for transmittance. The accuracy of V_0 was better than 1% on relatively stable and fine days. A calibration method for the near-infrared channels, 1225, 1627, and 2200 nm, was also developed. The logarithm of the ratio of the sensor output can be written as a linear function of the airmass, by assuming that the ratio of the optical thicknesses between the two channels is constant. The accuracy of V_0 was better than 1% on days with good conditions.

1. Introduction

Atmospheric aerosols are an important constituent of the atmosphere. Aerosols change the radiation budget directly by absorbing and scattering solar radiation and indirectly through their role as cloud condensation nuclei (CCNs), thereby increasing cloud reflectivity and lifetime (e.g., Ramanathan et al. 2001, Lohmann and Feichter 2005). Aerosols also affect human health as one of the main components of air pollution.

Atmospheric aerosols have a large variability in time and space. Therefore, measurement networks covering an extensive area on the ground and from space have been developed and established to determine the spatiotemporal distribution of aerosols related to climate forcing and air quality on multiple time scales and on regional, hemispheric, and global spatial scales.

Ground-based observation systems, such as those using radiometers, are more accurate and easier to install and maintain than space-based systems. Therefore, ground-based observation data are used to validate data obtained from space-based systems (Kahn et al. 2005, Remer et al. 2005, Mélin et al. 2010). Well-known ground-based networks include AERONT (AErosol RObotic NETwork) (Holben et al. 1998), SKYNET (Takamura and Nakajima 2004) and PFR-GAW (Precision Filter Radiometer-Global Atmosphere Watch) (Wehrli 2005).

In ground-based observation networks, direct solar irradiance and sky radiance are measured, and the aerosol characteristics are retrieved by analyzing these data: optical thickness, single scattering albedo, phase function, complex refractive index, and size distribution. To improve the measurement accuracy, it is important to know the characteristics of the instruments and to calibrate the instruments. Furthermore, from the view point of the validation of optical properties retrieved from the satellite measurement data, it is important to know the accuracy of the ground-based measurements.

In SKYNET, the radiometers POM-01 and POM-02, manufactured by Prede Co. Ltd., Japan, are used. These radiometers are called 'sky radiometers', and measure both the solar direct irradiance and sky-radiances. The objectives in this study are to investigate the current status of and problems with the sky radiometer.

There are two constants that we must determine to make accurate measurements. One is the calibration constant, and the other is the solid view angle (SVA) of the radiometer. The calibration constant is the output of the radiometer to the extra-terrestrial solar irradiance. The SVA is a constant which relates the sensor output to the sky radiance. The ambient temperature affects the sensor output, and this temperature dependence must be considered when analyzing data from POM-01 and POM-02. In this study, the temperature dependence of POM-02 and the calibration of the sensor are described. The SVA is described in detail in Part II.

In section 2, we briefly describe the data used in this study. In section 3, firstly, the temperature characteristics of POM-02 are described. Though the majority of POM-01 and POM-02 users do not explicitly consider the temperature dependence of the instruments, some channels have a large temperature dependence.

Secondly, the accuracy of the calibration constant is described for the sensor output for the extra-terrestrial solar irradiance. Most POM-01 and POM-02 users calibrate the sky radiometers with the Improved Langley (IML) method (Tanaka et al. 1986), because this method only needs on-site measurement data and special measurements for calibration are not required. One of the goals of this paper is to examine the accuracy of the IML method, but before that, in section 4, we consider the accuracy of the normal Langley method using the data obtained at NOAA Mauna Loa observatory (MLO), which is one of most suitable places for sky radiometer calibration by the normal Langley method, and the accuracy of the calibration constant obtained from side-by-side measurement. In section 5, though Campanelli et al. (2004) have already estimated the accuracy of the IML method, we estimate it again and show the time variation and the relation between the calibration constant and temperature dependence, and review the IML method. Then, in section 6, an example of the

Atmos. Meas. Tech. Discuss., https://doi.org/10.5194/amt-2017-432
Manuscript under review for journal Atmos. Meas. Tech.
Discussion started: 11 January 2018

Atmospheric Measurement Techniques Discussions

accuracy of the calibration using a calibrated integrating sphere is shown.

In SKYNET, the 940, 1627, and 2200 nm channels were not used. Therefore, the precipitable water vapor (PWV) and the optical thickness at 1627 nm are not estimated. However, these parameters are estimated in AERONET. In sections 7 and 8, calibration methods for these channels are shown using on-site measurement data. In section 9, the results are summarized.

2. Data

In this study, the measurements by two POM-02 sky radiometers which are used by the Japan Meteorological Agency/Meteorological Research Institute (JMA/MRI) were conducted. One is used as a calibration reference, POM-02 (Calibration reference), and the other is used for continuous measurement at the Tsukuba MRI observation site, POM-02 (Tsukuba).

To calibrate the reference POM-02 by the normal Langley method, the measurments were conducted at the NOAA Mauna Loa Observatory (MLO) for about one month every year, for more than twenty years. The MLO (19.5362°N, 155.5763°W) is located at an elevation of 3397.0 amsl on the northern slope of Mt. Mauna Loa, Island of Hawaii, Hawaii, USA. The atmospheric pressure is about 680 hPa. The MLO is one of the most suitable places to obtain data for a Langley plot and for a solar disk scan. Using these data, the calibration constant is estimated and the SVA is calculated.

The continuous observation was performed at the JMA/MRI (36.05°N, 140.13°E) in Tsukuba, which is located about 50 km northeast of Tokyo. Using these continuous measurement data, the calibration constants for the IML method were calculated using the SKYRAD software package (Nakajima et al. 1996, OpenCLASTR, http://www.ccsr.u-tokyo.ac.jp/~clastr/). Usually, the calibration of POM-02 for continuous measurement is conducted by comparison with the side-by-side measurement data from the reference POM-02.

The temperature dependence of the sensor output was measured using special equipment, which was originally used to measure the temperature dependence of the pyranometer. This equipment is managed and maintained by a branch of the JMA Observation Department.

3. Temperature dependence of sensor output

In this section, the temperature characteristics of the POM-02 are described. The POM-02 is temperature-controlled. However, the temperature control is insufficient. Therefore, the sensor output of the POM-02 is dependent on the environmental temperature.

The purpose of the temperature control is to keep the temperature inside the instrument from decreasing below levels which will reduce the instrument's accuracy. Instruments are usually designed to operate at temperatures either 20 or 30 ºC. When the temperature inside the instrument is below its threshold temperature (20 or 30 ºC), the instrument is heated. However, there is no cooling mechanism for when the temperature inside the instrument is higher than its threshold temperature for optimum operation. To monitor the temperature inside the instrument, a temperature sensor is attached near the filter turret. Furthermore, the near-infrared detector, which is thermoelectrically cooled, is equipped with a temperature sensor and temperature data can be recorded.

In Fig. 1, an example of the relation between the inside temperature of the instrument and the environmental temperature for POM-02 (Calibration Reference) is shown. The red line is the temperature near the filter turret and the blue line is the temperature of the near-infrared detector. The temperature control setting of this POM-02 is 20 ºC. The ambient temperature was varied in the order of 20, 0, −20, 0, 20, 40, 20 ºC. Since the mounting position of the temperature sensor and the thermal structure of the instrument were different for each product, not every POM-02 temperature responds in the same way.

In Fig. 2, the relation between the sensor output and the inside temperature near the filter turret for POM-02 (Calibration Reference) is shown. The sensor output is normalized by the sensor output at 20 ºC. The ambient environmental temperature was varied from −20 to 40 ºC. The detector used for wavelengths less than 1020 nm was a Si photodiode, and the detector for the 1225, 1627, and 2200 nm wavelengths was a thermoelectrically cooled InGaAs photodiode. In this study, the former wavelength region is referred to as the "visible region" and the latter one is the "near-infrared region".

The temperature dependence of the sensor output in the 340 and 2200 nm channels was larger than in the other channels. The range of the atmospheric temperature at Tsukuba was about −5 to 35 ºC, and the resulting inside temperatures were between 15 and 35 ºC (Fig. 1), with the change in the temperature less than 1.5% except for the 340 and 2200 nm channels. The temperature dependence of the sensor output varies with the channel.

In the 340 nm channel, the sensor output decreased by 7% when the internal temperature increased from 20 to 40 ºC. In the 2200 nm channel, the sensor output decreased by a rate of 5 to 6% per 10 degrees of temperature increase. Therefore, the

Atmos. Meas. Tech. Discuss., https://doi.org/10.5194/amt-2017-432
Manuscript under review for journal Atmos. Meas. Tech.
Discussion started: 11 January 2018

temperature dependence of the sensor output cannot be ignored in these two channels.

In Fig. 3, the temperature dependence of the sensor output for POM-02 (Tsukuba) is shown. The temperature dependence of the sensor output in the 340, 380, and 2200 nm channels is large for this POM-02. In the 340 and 380 nm channels, the rate of sensor output decrease was about 1.5% per 10 degrees, and in the 2200 nm channel, the rate of sensor output decrease was about 3% per 10 degrees. In the other channels, the temperature dependence of the sensor output was less than 1% for temperatures between 0 and 40 ºC.

Though only two examples were shown here, the temperature dependence of the sensor output differed between instruments. If we want to accurately consider the temperature dependence of the sensor output, we need to measure it for each instrument or only use channels with a small temperature dependence.

4. Normal Langley method

To determine the accuracy of the IML method, first the accuracies of the normal Langley method and the transfer of the calibration constant are investigated. The transferred calibration constant can be obtained by comparing the side-by-side measurement of the direct solar irradiance.

4.1 Accuracy of normal Langley method

Figure 4 shows an example of a Langley plot using the data obtained at MLO. In these Langley plots, the data in both the morning and afternoon are plotted. The linear regression lines were determined using the data with airmasses from 2 to 6 AM. From these examples, by using data taken at a location with suitable conditions, it is possible to determine an accurate calibration line.

At MLO, ten to twenty measurements for the Langley calibration can usually be taken over a period of 30 to 40 continuous observation days depending on the weather conditions. Near-infrared channels are more sensitive to weather conditions than channels in the visible range, because there are water vapor absorption bands in the near-infrared channel and the water vapor in the atmosphere tends to fluctuate.

Table 1 shows the calibration constants (V_0) determined using the data taken from October 2015 to November 2015 at MLO. The calibration constants were calculated for the following four cases.

Case 1, no gas absorption, and no temperature correction (NGABS, NTPC)

Case 2, no gas absorption, and temperature correction (NGABS, TPC)

Atmos. Meas. Tech. Discuss., https://doi.org/10.5194/amt-2017-432
Manuscript under review for journal Atmos. Meas. Tech.
Discussion started: 11 January 2018

Atmospheric Measurement Techniques Discussions

Case 3, gas absorption, and no temperature correction (GABS, NTPC)

Case 4, gas absorption, and temperature correction (GABS, TPC)

The error of the calibration constants ((SD)/V_0, SD: standard deviation, V_0 is the mean value) were 0.2 to 1.3% except in the 940 nm channel, where the mean V_0 and standard deviation were calculated from all data without weighting. If the weighted mean is used, a smaller error is expected: less than 1%. From these results, it can be seen that the calibration constant can be reliably determined by the normal Langley method using the data taken at MLO.

The effect of the temperature dependence is large in the 340 and 2200 nm channels, based on the ratio of (GABS,NTPC)/(GBAS,TPC) (= (Case 3)/(Case 4)). In the other channels, the effect of the temperature dependence is less than 0.9%. The range of the atmospheric temperature was about 5 to 15 °C when the measurements for the calibration at MLO were being conducted. Therefore, the effect of the temperature dependence on the sensor output is small.

From the ratio of (NGABS,TPC)/(GABS,TPC) (= (Case 2)/(Case 4)), the effect of gas absorption is more than 10% in the 940 nm channel, less than 0.4% in the 1225 and 1627 nm channels, and about 1% in the 2200 nm channel. These channels have weak gas absorption by water vapor, CO_2, and CO.

As seen from the ratio of (NGABS,NTPC)/(GABS,TPC) (= (Case 1)/(Case 4)), the calibration constants, except in the 340, 940, and 2200 nm channels, can be determined with an error of less than 1% without consideration of the temperature effect and gas absorption by using the data taken at MLO.

To calibrate the 940 nm channel, the vertical distribution of water vapor is necessary. The vertical distribution of water vapor is constructed with radiosonde data from the nearest site, precipitable water vapor (PWV) by the Global Positioning System (GPS), and relative humidity measured at MLO, and the transmittance is calculated (Uchiyama et al. 2014). The radiosonde measurements were taken twice a day, and the PWV by GPS were the 30-minute averages. The temporal resolution of these data is not high enough to accurately determine the vertical distribution of the water vapor, resulting in a large error in the calibration constant in the 940 nm channel.

Figure 5 shows the annual variation of the calibration constants (V_0) for POM-02 (Calibration Reference). The lens in the visible region (Si photodiode region) was replaced in 2013 and the interference filter in the 1225 nm channel was replaced in

2014. Since insufficient data were taken due to bad weather conditions in 2007 and 2008, the calibration could not be performed with sufficient accuracy. Therefore, the degradation is not smooth in some channels.

In general, the degradation at shorter wavelengths is larger than at longer wavelengths in the Si photodiode region. During the period from 2006 to 2013, the changes of V_0 in the 340, 380, and 400 nm channels were −10% per year, −7% per year, and −4% per year, respectively. The changes of V_0 in the 500, 675, and 870 nm channels were about −1% per year, and that in the 1020 nm channel was almost zero. These results indicate that calibration is necessary at least once a year to monitor the degradation of V_0.

The accuracy of the calibration in the near-infrared region is sensitive to weather conditions. Therefore, the annual variation of the calibration constant is not always smooth. However, from 2009 to 2013, the annual change of the calibration constant was less than 1%.

4.2 Accuracy of transfer by direct solar measurement

The calibration constant for one instrument can be used to estimate the calibration constant for another instrument by comparison with the simultaneous measurements of the solar direct irradiance.

Table 2 shows the results of the calibration constant transferred from POM-02 (Calibration Reference) to POM-02 (Tsukuba) and POM-02 (Fukuoka) in December 2014. The comparison measurements were conducted over 11 days for POM-02 (Tsukuba) and 8 days for POM-02 (Fukuoka). The error (SD/V_0) is 0.1 to 0.5% depending on the wavelength, where mean V_0 is the arithmetic mean. The error is 0.5% even for water vapor in the 940 nm channel; usually the fluctuation of the sensor output is large due to fluctuations in the water vapor amount. If the weighted mean is used as the expected value, a smaller error than that of the arithmetic mean is expected.

The observations for the comparison depend on the weather conditions, but if instruments are calibrated, it is the most straightforward and accurate way to transfer and determine the calibration constant for different instruments.

5. Improved Langley method

5.1 Comparison between Improved Langley and normal Langley method

In the Improved Langley (IML) method, the temperature dependence of the sensor output is not usually explicitly considered. This means that the calibration constant determined by the IML method implicitly includes the temperature dependence of the sensor output. Before comparing the calibration constant determined by the IML method and that transferred from POM-02 (Calibration Reference), we examined how much the sensor output changes with ambient temperature change.

In Fig. 6, the monthly mean values of the inside temperature of POM-02 (Tsukuba) and the temperature of the near-infrared detector are shown. As seen from the figure, these temperatures were controlled in the period from November to April. In Fig. 7, the temperature correction factors are shown, where the reference temperature is 20 °C. In the summer, the sensor output must be corrected by 1.5 to 2% in the 340 and 380 nm channels and by 4% in the 2200 nm channel. In the other channels, the corrections were less than 0.5%: the temperature effect on these channels was small.

In Fig. 8, the calibration constants determined by the IML method from January 2014 to December 2015 are shown. To compare between the IML and normal Langley methods, the calibration constants transferred from POM-02 (Calibration Reference) are also shown. The observations for the calibration transfer were conducted in December 2013, December 2014, and December 2015, and the calibration constants for POM-02 (Tsukuba) were determined. The calibration constants in other months were obtained by linear interpolation and the temperature correction factor was also taken into consideration. In Fig. 8, the running means of the monthly IML value are also shown.

For every channel, the calibration constants determined by the IML method have a seasonal variation: they are larger in the winter and smaller in the summer. The amplitude of the seasonal variation is larger than that of the temperature correction factor. Furthermore, the annual trend of the calibration constant, after removing the seasonal variation, is almost the same as by the normal Langley method.

In the 380 nm channel, the calibration constant changes due to the temperature dependence of the sensor output: in the summer the calibration constant decreases by about 2%. The calibration constant (V_0) determined by the IML method changes by up to 6%. Even if the effect of the temperature change is subtracted from the seasonal variation, there is a difference of about 4% between the calibration coefficients. In the

Atmos. Meas. Tech. Discuss., https://doi.org/10.5194/amt-2017-432
Manuscript under review for journal Atmos. Meas. Tech.
Discussion started: 11 January 2018

400, 500, 675, and 870 nm channels, there is a difference of 1 to 2% between the calibration coefficients, and in the 340 nm channel, there is a difference of 3% between the calibration coefficients. In the 1020 nm channel, since the interference filter was changed in September 2015, a direct comparison is difficult. In Table 3, the statistics of the difference between both calibration coefficients are shown. The RMS error is about 0.6 to 2.5% depending on the wavelength. This result is almost the same as in Campanelli et al. (2004). However, the maximum difference between both calibration coefficients was about 1.3 to 4.7%, and these differences are rather large. The statistics of the 3-point running mean for the IML method are also shown in Table 3. The errors are a bit smaller than for the non-smoothed values: the RMS error is about 0.5 to 1.7%.

Though the period of comparison is only two years, the calibration constant by the IML method represents the annual trend and implicitly includes the temperature dependence of the sensor output. However, the calibration constant has a seasonal variation of 1 to 3%, and in some cases, the maximum difference reaches about 5%. The 2% error in the calibration constant is not significant in a turbid atmosphere, but it is significant in a clear atmosphere, such as in polar and ocean regions. Furthermore, there is a possibility that the seasonal variation of the calibration constant causes an artificial seasonal variation in the retrieved parameters. The seasonal variation can be reduced by smoothing, such as with a running mean. However, over-smoothing dampens the temperature effect of the sensor output.

5.2 Review of Improved Langley method

In this section, the Improved Langley method is briefly reviewed and we examine possible issues with the IML method.

The solar direct irradiance at the surface based on the Beer-Bouguer-Lambert Law is written as follows:

$$F = F_0 \exp(-m\tau) \qquad (1)$$

where F and F_0 are the solar irradiance at the surface and the top of the atmosphere, respectively, $m = 1/\mu_0$ is the airmass, μ_0 is the cosine of the solar zenith angle, and τ is the layer optical thickness.

The single scattering by aerosol in the almucantar of the sun is given by the following equation:

Atmos. Meas. Tech. Discuss., https://doi.org/10.5194/amt-2017-432
Manuscript under review for journal Atmos. Meas. Tech.
Discussion started: 11 January 2018

$$\begin{aligned} I_1(\mu_0,\phi) &= m\tau\omega_0 P(\cos\Theta)F_0\exp(-m\tau) \\ &= m\tau_{sca}P(\cos\Theta)F_0\exp(-m\tau) \end{aligned} \quad (2)$$

where a one-layer plane-parallel atmosphere is assumed, $\tau_{sca} = \tau\omega_0$ is the layer scattering optical thickness, ϕ is the azimuthal angle measured from the solar principal plane, ω_0 is the single scattering albedo, and $P(\cos\Theta)$ is the normalized phase function at the scattering angle Θ. The Improved Langley method is based on these equations.

If the sensor output is proportional to the input energy, the following equation can be written for the direct solar measurement:

$$V = V_0\exp(-m\tau) \quad (3)$$

where $V = CF$, $V_0 = CF_0$, and C is the proportional constant (sensitivity). The contribution of scattered light in the field of view is ignored.

The sensor output for the measured single scattering V_1 can be written as follows:

$$\begin{aligned} V_1 &= CI_1(\mu_0,\phi)\Delta\Omega \\ &= Cm\tau\omega_0 P(\cos\Theta)F_0\exp(-m\tau)\Delta\Omega \\ &= m\tau\omega_0 P(\cos\Theta)V_0\exp(-m\tau)\Delta\Omega \end{aligned} \quad (4)$$

where $\Delta\Omega$ is the SVA.

From these equations, the following equations can be obtained:

$$m\tau = \frac{V_1}{\omega_0 P(\cos\Theta)V_0\exp(-m\tau)\Delta\Omega} \quad (5)$$

$$m\tau_{sca} = \frac{V_1}{P(\cos\Theta)V_0\exp(-m\tau)\Delta\Omega} \quad (6)$$

Then from eq. (3), we can get the following equations:

$$\ln V = \ln V_0 - m\tau \quad (7)$$

$$\ln V = \ln V_0 - m\tau_{sca}/\omega_0 \quad (8)$$

If m, $m\tau$, and $m\tau_{sca}$ can be obtained, the logarithm of the sensor output can be linearly fitted with m, $m\tau$, and $m\tau_{sca}$. The case when the x-axis is m and the

Atmos. Meas. Tech. Discuss., https://doi.org/10.5194/amt-2017-432
Manuscript under review for journal Atmos. Meas. Tech.
Discussion started: 11 January 2018

Atmospheric Measurement Techniques Discussions

y-axis is $\ln V$ corresponds to the normal Langley method, and the case when the x-axis is $m\tau$ or $m\tau_{sca}$ and the y-axis is $\ln V$ is the Improved Langley method. In the normal Langley method, the intersection of the y-axis and the regression line is $\ln V_0$ and the slope of the regression line is $-\tau$. There are two IML methods. If the x-axis is $m\tau$, the intersection of the y-axis and the regression line is $\ln V_0$ and the slope is -1. Otherwise, if the x-axis is $m\tau_{sca}$, the intersection of the y-axis and the regression line is $\ln V_0$ and the slope is $-1/\omega_0$. The SKYRAD package adopts the latter method.

In the SKYRAD package, two observable quantities are analyzed. One is the direct solar irradiance (eq. (3)), and the other is defined as

$$R(\lambda,\Theta) = \frac{V(\lambda,\Theta)}{V(\lambda,0)m\Delta\Omega} \tag{9}$$

where $V(\lambda,\Theta)$ is the sensor output of the sky radiance measurement for the scattering angle Θ, $\cos\Theta = \mu_0^2 + (1-\mu_0^2)\cos\phi$, $\Delta\Omega$ is the SVA of the sky radiometer, and $V(\lambda,0)$ is the direct solar irradiance. This is the sky radiance normalized by the direct solar irradiance.

$V(\lambda,\Theta)$ is composed of the single scattering and multiple scattering radiances. Therefore, eq. (9) can be expressed as follows:

$$\begin{aligned} R(\lambda,\Theta) &= \frac{V_1(\lambda,\Theta)}{V(\lambda,0)m\Delta\Omega} + R_m(\lambda,\Theta) \\ &= \tau\omega_0 P(\cos\Theta) + R_m(\lambda,\Theta) \end{aligned} \tag{10}$$

In the SKYRAD package, in the retrieval process for the Improved Langley method the single scattering and multiple scattering components are estimated by solving the radiative transfer equation. Once the single scattering component is retrieved, $m\tau$ and $m\tau_{sca}$ are estimated. In the SKYRAD package, the complex refractive indexes for each channel are given and the measurement data with a scattering angle of less than 30 degrees are used.

Once $m\tau$ is obtained, the calibration constants can be estimated from $\ln V_0 = \ln V + m\tau$. However, in the SKYRAD package, $\ln V_0$ and W_0 are determined

Atmos. Meas. Tech. Discuss., https://doi.org/10.5194/amt-2017-432
Manuscript under review for journal Atmos. Meas. Tech.
Discussion started: 11 January 2018

by fitting to $\ln V = \ln V_0 - m\tau_{sca} / W_0$. In eq. (8), W_0 is the single scattering albedo. The single scattering albedo is defined as the ratio of the scattering coefficient to the extinction coefficient. Therefore, the single scattering albedo must be a value between zero and one. However, W_0 is frequently greater than 1. The fitted error, number of measurements, and the transmittance are checked. Then, the data passing the check criterion are chosen as the calibration constants.

For the 500 nm channel, Figs. 9 shows a scatter plot of V_0 and the optical thickness at 500 nm, a scatter plot of W_0 and V_0, and (c) a time series of V_0 from January 2014 to December 2015. In this case, the V_0 values with errors less than 0.01 were chosen. Figure 9 (a) shows that there is no dependence of V_0 on the optical thickness. Also, there is no dependence of V_0 on the Ångström exponent (not shown). Figure 9 (b) shows that V_0 and W_0 are negatively correlated, and that even if the correct W_0 is determined, the V_0 are scattered with a width of about 4%. Figure 9 (c) also shows that V_0 is determined to within about a 2% uncertainty and that V_0 has a seasonal variation. These figures show that the V_0 determined by the IML method in the SKYRAD package has a 2% uncertainty.

As stated above, V_0 can be determined from $\ln V_0 = \ln V + m\tau$. However, the V_0 determined from this equation are systematically overestimated by several percent and have a larger seasonal variation than by linear fitting to $\ln V = \ln V_0 - m\tau_{sca} / W_0$.

In the Improved Langley method, the refractive index is fixed. This causes the estimation error in the single and multiple scattering in eq. (10). This may also be the cause of the 2% uncertainty. Some iterative process may be necessary to reduce this uncertainty.

Atmos. Meas. Tech. Discuss., https://doi.org/10.5194/amt-2017-432
Manuscript under review for journal Atmos. Meas. Tech.
Discussion started: 11 January 2018

Atmospheric Measurement Techniques Discussions

6. Calibration using the calibrated light source

In this section, the accuracy of the calibration using the calibrated integrating sphere is described. If POM-02 can be calibrated using the calibrated light source, then POM-02 can be calibrated quickly without being influenced by the weather.

In this study, the integrating sphere, which is calibrated and maintained by the Japanese Aerospace Exploration Agency (JAXA), was used (Yamamoto et al. 2002). This integrating sphere is used to calibrate the radiometers which are used to validate satellite remote sensing products.

To use the light source, the extra-terrestrial solar irradiance and the SVA of the sky radiometer are necessary, as well as the radiance emitted by the light source. The extra-terrestrial solar irradiance by Gueymard (2004) was used here, along with the SVA obtained by processing the solar disk scan data.

When the integrating sphere is measured by POM-02, the sensor output is written as follows:

$$V_{sph}(\lambda_0) = \int_{\Delta\lambda} C(\lambda)\varphi(\lambda)I_{sph}(\lambda)d\lambda \cdot \Delta\Omega \Big/ \int_{\Delta\lambda} \varphi(\lambda)d\lambda \quad (11)$$

where $V_{sph}(\lambda_0)$ is the sensor output in channel λ_0, $C(\lambda)$ is the sensitivity at wavelength λ, $\varphi(\lambda)$ is the spectral response function of the interference filter, $I_{sph}(\lambda)$ is the spectral radiance from the integrating sphere at wavelength λ, and the emitted radiance from the integrating sphere is assumed to be homogeneous. This equation is approximated as follows:

$$V_{sph}(\lambda_0) \cong C(\lambda_0)\bar{I}_{sph}(\lambda_0) \cdot \Delta\Omega \quad (12)$$

where

$$\bar{I}_{sph}(\lambda_0) = \int_{\Delta\lambda} \varphi(\lambda)I_{sph}(\lambda)d\lambda \Big/ \int_{\Delta\lambda} \varphi(\lambda)d\lambda \quad (13)$$

When the extra-terrestrial solar irradiance is measured, the sensor output is written as follows:

$$V_{sun}(\lambda_0) = \int_{\Delta\lambda} C(\lambda)\varphi(\lambda)F_0(\lambda)d\lambda \Big/ \int_{\Delta\lambda} \varphi(\lambda)d\lambda \quad (14)$$

where $V_{sun}(\lambda_0)$ is the sensor output in channel λ_0, and $F_0(\lambda)$ is the extra-terrestrial solar spectral irradiance. This equation is approximated as follows:

Atmos. Meas. Tech. Discuss., https://doi.org/10.5194/amt-2017-432
Manuscript under review for journal Atmos. Meas. Tech.
Discussion started: 11 January 2018

Atmospheric Measurement Techniques Discussions

$$V_{sun}(\lambda_0) \cong C(\lambda_0)\overline{F}_0(\lambda_0) \tag{15}$$

where

$$\overline{F}_0(\lambda_0) = \int_{\Delta\lambda} \varphi(\lambda)F_0(\lambda)d\lambda \bigg/ \int_{\Delta\lambda} \varphi(\lambda)d\lambda \tag{16}$$

From eqs. (12) and (15), $V_{sun}(\lambda_0)$ is written as follows:

$$V_{sun}(\lambda_0) \cong V_{sph}(\lambda_0)\frac{\overline{F}_0(\lambda_0)}{\overline{I}_{sph}(\lambda_0)\cdot\Delta\Omega} \tag{17}$$

In Table 4, the calibration constants for POM-02 (Calibration Reference) determined from the integrating sphere measurement are compared with the results of the Langley method. At POM-02 (Calibration Reference), the relative difference was 0.7 to 7.6% in channels 2 to 8, and 0.5 to 1.8% in channels 9 to 11. The integrating sphere used in channels 2 to 8 is different from that in channels 9 to 11.

The value of the extra-terrestrial solar spectrum is dependent on the database. In Fig. 10, three data sets are shown (Thuillier et al. 2003, Gueymard 2004, and 1985 Wehrli Standard Extraterrestrial Solar Irradiance Spectrum (Wehrli 1985, Neckel and Labs 1981)). The ratios of the solar spectrum to Gueymard (2004) are also shown. These figures show that there is a several percent difference in the values depending on the wavelength. The SVA error is 1% (see Part II); the disk scan data were taken at MLO, where measurement conditions were good for the solar disk scan. The accuracy of the integrating sphere was 1.7% (Yamamoto et al. 2002). Considering the magnitude of these errors, the above differences in the calibration constants seem reasonable. However, to reduce the optical thickness error below 0.01, a calibration coefficient error of several percent is too large. For estimating the optical thickness from measurements of the direct solar irradiance, the calibration coefficient determined by the Langley method is better.

7. Calibration of 940 nm channel

The calibration constant depends on the extra-terrestrial solar irradiance in the 940 nm band, the spectral response function of the interference filter, the spectral sensitivity of the detector, and the transmittance of radiometer optics. Calibration methods for the 940 nm channel, which is in the water vapor absorption band, have been considered extensively in previous studies (Reagan et al. 1987a, 1987b, 1995; Bruegge et al. 1992; Thome et al. 1992, 1994; Michalsky et al. 1995, 2001; Schmid et al.

Atmos. Meas. Tech. Discuss., https://doi.org/10.5194/amt-2017-432
Manuscript under review for journal Atmos. Meas. Tech.
Discussion started: 11 January 2018

Atmospheric Measurement Techniques Discussions

1996, 2001; Shiobara et al. 1996; Halthore et al. 1997; Cachorro et al. 1998; Plana-Fattori et al. 1998, 2004; Ingold et al. 2000; Kiedron et al. 2001, 2003). For example, Uchiyama et al. (2014) developed the Langley method which takes account of the gas absorption, and the empirical relationship between the transmittance and precipitable water vapor (PWV) was determined from the theoretical calculation by giving the spectral response function and the model atmosphere. The PWV is estimated from the transmittance for the 940 nm channel. The empirical formula is usually used for the transmittance of the 940 nm channel by water vapor.

Most POM-02 users have taken measurements without calibrating the 940 nm channel for a long time. To make use of these accumulated data, it is necessary to develop a calibration method using data at the observation site. Campanelli et al. (2014) developed a method to determine the calibration constant and parameters for the empirical formula of the transmittance using the on-site surface meteorological data and simultaneous POM-02 data. However, it is difficult to obtain the empirical formula for transmittance by the column water vapor from the surface measurement data.

In this study, given the spectral response function, the empirical transmittance formula is produced by the method shown in Uchiyama et al. (2014). Then, the modified Langley method shown below is performed using the empirical formula and the observation data.

The water vapor transmittance is approximated as follows:

$$Tr(\mathrm{H2O}) = \exp(-a(pwv)^b) \tag{18}$$

where a and b are fitting coefficients (see Appendix), and pwv is PWV.

The sensor output V is written as follows (Uchiyama et al. 2014):

$$\begin{aligned} V &= \frac{V_0}{R^2}\exp(-m(\tau+\tau_R))Tr(\mathrm{H2O}) \\ &= \frac{V_0}{R^2}\exp(-m(\tau+\tau_R))\exp(-a(m\cdot pwv)^b) \end{aligned} \tag{19}$$

where V_0 is the calibration coefficient, R is the distance between the earth and the sun, τ is the aerosol optical thickness at 940 nm, and τ_R is the optical thickness of the molecular scattering (Rayleigh scattering). The aerosol optical thickness τ at 940 nm is interpolated from the optical thicknesses at 870 and 1020 nm.

The above equation can be rewritten as follows:

Atmos. Meas. Tech. Discuss., https://doi.org/10.5194/amt-2017-432
Manuscript under review for journal Atmos. Meas. Tech.
Discussion started: 11 January 2018

Atmospheric Measurement Techniques Discussions

$$\ln VR^2 + m(\tau - \tau_R) = \ln V_0 - a(pwv)^b m^b \tag{20}$$

The parameters on the left-hand side are known: V is the measurement value, R and m can be calculated from the solar zenith angle, and τ_R is estimated from the surface pressure. If pwv is constant, then the right-hand side of the equation is a linear function of m^b. Therefore, the values on the left-hand side can be fitted by a linear function of m^b, and the intersection of the y-axis and the fitted line is $\ln V_0$.

Before the above-mentioned method was applied to the MRI data, it was first applied to the data taken at MLO, which has more stable weather conditions than Tsukuba, MRI. The results applied to the data taken at MLO in October and November 2014 and in October and November 2015 are shown in Table 5.

The calibration coefficients determined in 2014 and 2015 were 2.2973×10^{-4} (SD/V_0=0.052) and 2.2954×10^{-4} (SD/V_0=0.047), respectively.

The calibration coefficients determined by the Langley method with consideration of gas absorption in 2014 and 2015 were 2.3364×10^{-4} (SD/V_0=0.093) and 2.3157×10^{-4} (SD/V_0=0.097), respectively. Though there are differences of 1.7% and 0.9%, these values are very similar. The error of the new method is smaller than the method which takes account of gas absorption more accurately than the new method. This may be due to errors in the estimates of the water vapor amount and distribution: the PWV is obtained from the GPS PWV, which has a low time resolution (30-minute average) and some data are missing, and the vertical distribution is estimated from only two radiosonde measurements per day near MLO.

The water vapor amount tends to fluctuate. Though the restriction that the PWV be constant is severe, the above method is applied to the data taken at Tsukuba, MRI and the calibration constants are compared with the calibration constant for POM-02 (Calibration Reference), which was calibrated by the Langley method with consideration of the gas absorption using the data taken at MLO and interpolated to the observation day (see Table 6).

The ratio of the calibration coefficients in the period from December 14, 2014 to January 5, 2015 (10 cases) was 1.0094, and in the period December 1, 2015 to December 30, 2015 (17 cases) it was 0.99818. Thus, the difference between the two methods is less than 1%.

Although it seems that the above-mentioned modified Langley method does not work well at all locations and under all weather conditions, the calibration constant of the 940 nm channel can be determined by applying the above-mentioned method on a relatively stable and fine day at the observation site.

8. Calibration coefficients of near-infrared channels

The measurements for the near-infrared channels, 1225, 1627, and 2200 nm, of POM-02 have been performed at many SKYNET sites, but the data have not been analyzed, because most POM-02 users cannot calibrate these channels by themselves.

These channels can be calibrated with the Langley method with a reasonable accuracy by taking into account the gas absorption. However, many users cannot make these measurements for the Langley method. Furthermore, the scattering of light in these channels is small and the IML method cannot be applied.

For some observation days, data with a very high correlation between channels may be obtained. In this case, if the calibration constant of one channel is known, then the calibration constants of the other channels can be inferred. The general method for the case when the ratio of the optical thicknesses is constant was shown by Forgan (1994).

In this study, by assuming that the channels in the visible region including the 940 nm channel are calibrated, a similar method was applied to the near-infrared channels to determine the calibration constant and the accuracy was investigated.

The sensor output of POM-02 is written as follows:

$$V = \frac{V_0}{R^2}\exp(-m(\tau + \tau_R))Tr(gas) \tag{21}$$

where V is the sensor output, V_0 is the calibration constant, R is the distance between the earth and the sun, m is the airmass, τ is the aerosol optical thickness, τ_R is the optical thickness of the molecular scattering (Rayleigh scattering), and $Tr(gas)$ is the transmittance of the gas absorption.

The sensor output for channels 1 and 2 are as follows:

$$V_1 = \frac{V_{01}}{R^2}\exp(-m(\tau_1 + \tau_{R1}))Tr_1(gas) \tag{22}$$

$$V_2 = \frac{V_{02}}{R^2}\exp(-m(\tau_2 + \tau_{R2}))Tr_2(gas)\,. \tag{23}$$

The calibration constant of channel 1 is assumed to be known and that of channel 2 is determined.

Atmos. Meas. Tech. Discuss., https://doi.org/10.5194/amt-2017-432
Manuscript under review for journal Atmos. Meas. Tech.
Discussion started: 11 January 2018

Atmospheric Measurement Techniques Discussions

From eqs. (22) and (23), the following equation is obtained:

$$\frac{V_2}{V_1} = \frac{V_{02}\exp(-m(\tau_2 + \tau_{R2}))Tr_2(gas)}{V_{01}\exp(-m(\tau_1 + \tau_{R1}))Tr_1(gas)}$$

Therefore,

$$\ln\frac{V_2}{V_1} = \ln\frac{V_{02}}{V_{01}} - m(\tau_2 - \tau_1) - m(\tau_{R2} - \tau_{R1}) + \ln\frac{Tr_2(gas)}{Tr_1(gas)} \qquad (24)$$

$$\begin{aligned}\ln\frac{V_2}{V_1} + m(\tau_{R2} - \tau_{R1}) - \ln\frac{Tr_2(gas)}{Tr_1(gas)} &= \ln\frac{V_{02}}{V_{01}} - m(\tau_2 - \tau_1) \\ &= \ln\frac{V_{02}}{V_{01}} - (\frac{\tau_2}{\tau_1} - 1)\tau_1 m\end{aligned} \qquad (25)$$

If the water vapor amount is estimated from the 940 nm channel, and the mixing ratio of CO_2 and CO is given, then the transmittance of gas can be estimated. Given the observation time and the latitude and longitude of the observation site, the airmass is calculated, and τ_{R1} and τ_{R2} are calculated from the surface pressure. Therefore, the left-hand side of eq. (25) is known. Furthermore, if the ratio of the optical thickness τ_2/τ_1 is constant, then this equation is a linear function of $m\tau_1$. Therefore, the intersection of the y-axis and the linearly fitted line is $\ln V_{02}/V_{01}$, and if V_{01} is known, then V_{02} is also known. Although this condition is not always satisfied, sometimes a linear fit will provide sufficient accuracy.

This method was applied to the data of POM-02 (Calibration Reference) from December 2014 to December 2015. The 500 nm was chosen as channel 1 in eq. (25). The data used here had an RMS error of 0.005. In Fig. 11(a), the monthly mean of V_{02}/V_{01} and the standard deviation are shown. The lines of the ratio, which are interpolated from the calibration constant determined using the data taken in October and November of 2014 and 2015 at MLO, are also shown. In Fig. 11 (b), the ratio of the calibration constant by the above method and the interpolated value of the calibration constant determined from the MLO data are shown. In the 1627 nm channel, the differences are less than 2% throughout the year and the differences in December and January are less than 1%. In the 1225 nm channel, the differences are less than 2% except in April 2015. In the 2200 nm channel, the differences in some months are more than 3%. However, in December 2015, the differences in all channels are less than 1%. This shows that the calibration constant can be determined by the method shown here to within an accuracy of 1% under suitable conditions. Currently, there is no method to calibrate the near-infrared channel from on-site observation data. The method shown here is an alternative to the Langley method.

9. Summary and conclusion

Atmospheric aerosols are an important constituent of the atmosphere. Measurement networks covering an extensive area from ground and space have been developed to determine the spatiotemporal distribution of aerosols. SKYNET is a ground-based monitoring system using sky radiometers POM-01 and POM-02 manufactured by Prede Co. Ltd., Japan. To improve their measurement accuracy, it is important to know the characteristics of the instruments and accurately calibrate them accordingly.

There are two constants that we must determine to make accurate measurements. One is the calibration constant, and the other is the SVA of the radiometer. Additionally, the temperature dependence of the sensor output is another important characteristic.

In this study, the data obtained by two sky radiometers POM-02 of the JMA/MRI are considered. One of the sky radiometers is used as a calibration reference, and the other is used for continuous measurement at the Tsukuba MRI observation site.

The sensor output of POM-02 is dependent on the environmental temperature. The temperature dependence of the sensor output in the 340, 380, and 2200 nm channels was larger than in other channels. For example, the sensor output in the 340 and 380 nm channels of POM-02 (Tsukuba) increased at a rate of about 1.5% per 10 degrees, and that in the 2200 nm channel increased at a rate of about 3% per 10 degrees. In the other channels, the sensor output increased at a rate of less than 1% when the sensor's internal temperature was 0 to 40 ºC. The temperature dependence of the two POM-02 examined here was different for each instrument. If we want to make accurate measurements, we need to measure the temperature dependence for each instrument or use the channels with a small temperature dependence.

For the measurement at Tsukuba, the temperature inside the POM-02 (Tsukuba) was controlled during the winter and spring seasons from November to April, but was not regulated, and thus was high during the summer. In the summer, sensor output must be corrected by 1.5 to 2% in the 340 and 380 nm channels and by 4% in the 2200 nm channel. In the other channels, the corrections were less than 0.5%.

As well as determining the accuracy of the IML method, this study investigated the accuracy of the normal Langley method and of the calibration transfer. From the data taken at MLO, the error in the calibration constants determined by the normal Langley method (SD/V_0) was 0.2 to 1.3%, except in the 940 nm channel. The effect of

Atmospheric Measurement Techniques Discussions
Open Access EGU

gas absorption was more than 10% in the 940 nm channel, but was less than 0.4% in the 1225 and 1627 nm channels and less than 1% in the 2200 nm channel, which all have weak gas absorption.

The comparison measurements for transferring the calibration constant were conducted in December at Tsukuba over about ten days. The error (SD/V_0) for the transfer method was 0.1 to 0.5% depending on the wavelength. Though the measurements for the comparison depend on the weather conditions, if there are calibrated instruments, then it is a straightforward and accurate way to determine the calibration constant.

The annual variation of the calibration constants (V_0) for POM-02 (Calibration Reference) was also investigated. Roughly speaking, the degradation in the shorter wavelengths was larger than that in the longer wavelengths in the Si photodiode region. The changes in the 340 nm channel were −10% per year from 2006 to 2013. The change in the near-infrared region (thermoelectrically cooled InGaAs photodiode) was less than 1% from 2009 to 2013. These results indicate that calibration of the instruments is necessary at least once a year to monitor the degradation of V_0.

The calibration constant determined by the IML method and that transferred from the POM-02 (Calibration Reference) were compared using the data taken at Tsukuba from December 2013 to December 2015.

For every channel, the calibration constants determined by the IML method had a seasonal variation of 1 to 3%. The calibration constants determined by the IML method implicitly include the temperature dependence of the sensor output. However, even if the change due to the temperature variation is subtracted from the seasonal variation, there is a difference of 1 to 4% between the two calibration coefficients. The RMS errors of the differences between the two calibration coefficients were about 0.6 to 2.5%. This result is almost the same as that of Campanelli et al. (2004). However, in some cases, the maximum difference reached up to 5%. Furthermore, the annual trend of the calibration constant excluding the seasonal variation was almost the same as for the normal Langley method.

The IML method was reviewed and its error characteristics were investigated. There was no dependence of V_0 on the optical thickness and Ångström exponent, and V_0 and W_0 were negatively correlated. Furthermore, even if the optical thickness and

Atmos. Meas. Tech. Discuss., https://doi.org/10.5194/amt-2017-432
Manuscript under review for journal Atmos. Meas. Tech.
Discussion started: 11 January 2018

Atmospheric Measurement Techniques Discussions

W_0 are determined, the V_0 had an uncertainty of ±2%. The time series of V_0 showed a seasonal variation with an uncertainty of ±2%. These results show that the V_0 determined by the IML method using the SKYRAD package has about a ±2% uncertainty.

We also tried to determine V_0 using the calibrated integrating sphere as the light source. The relative differences of V_0 were about 1 to 8% depending on the wavelength. Considering the magnitude of the errors in the extra-terrestrial solar spectrum, SVA, and the integrating sphere, the above differences in the calibration constants seem reasonable. However, to reduce the optical thickness error below 0.01, an error of several percent in the calibration coefficient is too large.

The calibration method for water vapor channel in the 940 nm was developed using the on-site measurement data. V_0 was determined by the modified Langley method using a pre-determined empirical transmittance equation. The differences in the calibration coefficients between the normal Langley method and the above method were less than 1% on relatively stable and fine days.

The calibration method for the near-infrared 1225, 1627, and 2200 nm channels was also developed using the on-site measurement data. It is assumed that channels in the visible wavelength region and the 940 nm channel are calibrated. Then, if the ratio of the optical thicknesses between two channels is constant, the logarithm of the ratio of the sensor output can be written as a linear function of the airmass. Here, the calibration constant for one of the two channels is known and the transmittance of water vapor is calculated using the PWV estimated from the 940 nm channel. By fitting the logarithm of the ratio of sensor output to a linear function of the airmass, the ratio of the calibration constants is determined. By this method, the calibration constants could be determined to an accuracy of within 1% on the days with good weather conditions.

In this study, it is shown that some channels have a non-negligible temperature dependence in the sensor output and that the calibration constants determined by the IML method showed a seasonal variation and had an uncertainty of ±2%. In one channel, the maximum error reached about 5%. Reducing the uncertainty of the IML method is a task for future work, along with the problems related to the determination

Atmos. Meas. Tech. Discuss., https://doi.org/10.5194/amt-2017-432
Manuscript under review for journal Atmos. Meas. Tech.
Discussion started: 11 January 2018

of calibration constants. In particular, the calibration constants for the 940 nm channel and the near-infrared channels must be determined using on-site measurement data.

Appendix

Coefficients of water vapor transmittance.

Details of the method for determining the coefficients a and b are described in Uchiyama et al. (2014). The coefficients a and b depend on the vertical structure of the atmospheric temperature and humidity. Therefore, it is difficult to choose suitable values that can be applied under all atmospheric conditions. The range of variability of transmittance for an atmospheric profile is limited. Atmospheric transmittance is computed for a broad range of atmospheric conditions, and values for a and b were chosen that best fit the ensemble conditions.

The value of coefficients determined by our method for POM-02 (Calibration Reference) are a = 0.139186, b = 0.631. The values of the coefficients for the trapezoidal spectral response function, which has full width at a half maximum of 10 nm and central wavelength of 940 nm, are a =0.147101, b =0.625.

Acknowledgements

This work was supported by the NIES GOSAT-2 project, Japan. This work was partially supported by JSPS KAKENHI Grant Number JP17K00531.

References

Bruegge, C. J., J. E. Conel, R. O. Green, J. S. Margolis, R. G. Holm, and G. Toon, 1992: Water vapor column abundance retrievals during FIFE, *J. Geophys. Res.*, **97**, 18,759–18,768.

Cachorro, V. E., P. Utrillas, R. Vergaz, P. Duran, A. M. de Frutos, and J. A. Martinez-Lozano, 1998: Determination of the atmospheric-water-vapor content in the 940-nm absorption band by use of moderate spectral-resolution measurements of direct solar irradiance. *Appl. Opt.*, **37**, 4678–4689.

Campanelli, M., T. Nakajima, P. Khatri, T. Takamura, A. Uchiyama, V. Estellés G. L. Liberti, V. Malvestuto, 2014: Retrieval of characteristic parameters for water vapour transmittance in the development of ground based Sun-Sky radiometric measurements of columnar water vapour, *Atmos. Meas. Tech.*, **7**, 1075–1087, doi:10.5194/amt-7-1075-2014

Campanelli, M, T. Nakajima, and B. Olivieri, 2004: Determination of the solar calibration constant for a sun-sky radiometer: proposal of an *in-situ* procedure, *App.*

Atmos. Meas. Tech. Discuss., https://doi.org/10.5194/amt-2017-432
Manuscript under review for journal Atmos. Meas. Tech.
Discussion started: 11 January 2018

Atmospheric Measurement Techniques Discussions

Opt., **43**, 651-659.

Forgan, B.W., 1994: General method for calibrating Sun photometers, *App. Opt.*, **33**, 4841-4850.

Gueymard, C.A., 2004: The sun's total and spectral irradiance for solar energy applications and solar radiation models, *Solar Energy*, **76**, 423-453.

Halthore, R. N., T. F. Eck, B. N. Holben, and B. L. Markham, 1997: Sun photometric measurements of atmospheric water vapor column abundance in the 940-nm band. *J. Geophys. Res.*, **102**(D4), 4343–4352, doi:10.1029/96JD03247.

Holben, B. N., T. F. Eck, I. Slutsker, D. Tanré, J. P. Buis, A. Setzer, E. Vermote, J. A. Reagan, Y. J. Kaufman, T. Nakajima, F. Lavenu, I. Jankowiak, and A. Smirnov, 1998: AERONET-A federated instrument network and data archive for aerosol characterization. *Remote Sens. Environ.*,**66**, 1-16.

Ingold, T., B. Schmid, C. Matzler, P. Demoulin, and N. Kampfer, 2000: Modeled and empirical approaches for retrieving columnar water vapor from solar transmittance measurements in the 0.72, 0.82, and 0.94 μm absorption bands. *J. Geophys. Res.*, **105**, 24,327–24,343.

Kiedron, P., J. Michalsky, B. Schmid, D. Slater, J. Berndt, L. Harrison, P. Racette, E. Westwater, and Y. Han, 2001: A robust retrieval of water vapor column in dry Arctic conditions using the rotating shadowband spectroradiometer. *J. Geophys. Res.*, **106**, 24,007– 24,016.

Kiedron, P., J. Berndt, J. Michalsky, and L. Harrison, 2003: Column water vapor from diffuse irradiance. *Geophys. Res. Lett.*, **30**(11), 1565, doi:10.1029/2003GL016874.

Kahn, R. A, B. J. Gaitley, J. V. Martonchik, D. J. Diner, K. A. Crean, and B. N. Holben, 2005: Multiangle Imaging Spectroradiometer (MISR) global aerosol optical depth validation based on 2 years of coincident Aerosol Robotic Network (AERONET) observations, *J. Geophys. Res.*, **110**, D10S04. doi:10.1029/2004JD004706.

Lohmann, U., and J. Feichter, 2005: Global indirect aerosol effects: a review. *Atmos. Chem. Phys.*, **5**, 715-737.

Mélin, F., M. Clerici, G. Zibordi, B.N. Holben, A. Smirnov, 2010: Validation of SeaWiFS and MODIS aerosol products with globally distributed AERONET data, *Remote Sens. Environ.*, **114**, 230–250.

Michalsky, J. J., J. C. Liljegren, and L. C. Harrison, 1995: A comparison of sun photometer derivations of total column water vapor and ozone to standard measures of same at the Southern Great Plains atmospheric radiation measurement site. *J. Geophys. Res.*, **100**, 25,995–26,003.

Michalsky, J. J., Q. Min, P. W. Kiedron, D. W. Slater, and J. C. Barnard, 2001: A

Atmospheric Measurement Techniques Discussions
Open Access
EGU

differential technique to retrieve column water vapor using sun radiometry. *J. Geophys. Res.*, **106**, 17,433–17,442.

Nakajima, T., G. Tonna, R. Rao, Y. Kaufman, and B. Holben, 1996: Use of sky brightness measurements from ground for remote sensing of particulate polydispersions, *Appl. Opt.*, **35**, 2672–2686.

Neckel, H. and D. Labs, 1981: Improved Data of Solar Spectral Irradiance from 0.33 to 1.25 µm, *Sol. Phy.*, **74**, 231-249, doi:10.1007/BF00151293.

Plana-Fattori, A., M. Legrand, D. Tanre, C. Devaux, A. Vermeulen, and P. Dubuisson, 1998: Estimating the atmospheric water vapor content from sun photometer measurements. *J. Appl. Meteorol.*, **37**, 790– 804.

Plana-Fattori, A., P. Dubuisson, B. A. Fomin, and M. de Paula Correa, 2004: Estimating the atmospheric water vapor content from multi-filter rotating shadow-band radiometry at Sao Paulo, Brazil. *Atmos. Res.*, **71**, 171– 192

Ramanathan, V., P. J. Crutzen, J. T. Kiehl, and D. Rosenfeld, 2001: Aerosols, Climate, and the Hydrological Cycle. *Science*, **294**, 2119-2124.

Reagan, J. A., K. Thome, B. Herman, and R. Gall, 1987a: Water vapor measurements in the 0.94 micron absorption band-Calibration, measurements and data applications. *in Proc. Int. Geoscience and Remote Sensing '87 Symposium, Ann Arbor, Michigan, IEEE,* pp. 63–67.

Reagan, J. A., P. A. Pilewskie, B. M. Herman, and A. Ben-David, 1987b: Extrapolation of Earth-based solar irradiance measurements to exoatmospheric levels for broad-band and selected absorption-band observations. *IEEE Trans. Geosci. Remote Sens.*, **25**, 647–653.

Reagan, J., K. Thome, B. Herman, R. Stone, J. DeLuisi, and J. Snider, 1995: A comparison of columnar water vapor retrievals obtained with near-IR solar radiometer and microwave radiometer measurements. *J. Appl. Meteorol.*, **34**, 1384–1391.

Remer, L.A., Y.J. Kaufman, D. Tanré, S. Mattoo, D.A.Chu, J.V. Martins, R.-R. Li, C. Ichoku, R.C. Levy, R.G. Kleidman, F.F. Eck, E. Vermote, and B.N. Holben. 2005: The MODIS Aerosol Algorithm, Products, and Validation, *J. Atmos. Sci.*, **62**, 947-973.

Schmid, B., K. J. Thome, P. Demoulin, R. Peter, C. Matzler, and J. Sekler, 1996: Comparison of modeled and empirical approaches for retrieving columnar water vapor from solar transmittance measurements in the 0.94-µm region. *J. Geophys. Res.*, **101**, 9345–9358.

Schmid, B., J. J. Michalsky, D. W. Slater, J. C. Barnard, R. N. Halthore, J. C. Liljegren, B. N. Holben, T. F. Eck, J. M. Livingston, P. B. Russell, T. Ingold, and I. Slutsker, 2001: Comparison of columnar water-vapor measurements from solar transmittance methods, Appl. Opt., 40, 1886–1896.

Shiobara, M., J. D. Spinhirne, A. Uchiyama, and S. Asano, 1996: Optical depth measurements of aerosol, cloud, and water vapor using sun photometers during FIRE Cirrus IFO II. *J. Appl. Meteorol.*, **35**, 36–46.

Takamura, T, T. Nakajima and SKYNET community group, 2004: Overview of SKYNET and its Activities. Proceedings of AERONET workshop. *El Arenosillo. Optica Pura y Aplicada,* **37**, 3303–3308.

Tanaka, M., T. Nakajima, and M. Shiobara, 1986: Calibration of a sunphotometer by simultaneous measurements of direct-solar and circumsolar radiations, *Appl., Opt.*, **25**, 1170-1176.

Thome, K., B. M. Herman, and J. A. Reagan, 1992: Determination of precipitable water from solar transmission. *J. Appl. Meteorol.*, **31**, 157-165.

Thome, K. J., M. W. Smith, J. M. Palmer, and J. A. Reagan, 1994: Three-channel solar radiometer for the determination of atmospheric columnar water vapor. *Appl. Opt.*, **33**, 5811 –5819.

Thuillier, G., M. Hersé, D. Labs, T. Foujols, W. Peetermans, D. Gillotay, P.C. Simon, and H. Mandel, 2003: The solar spectral irradiance from 200 to 2400nm as measured by the SOLSPEC spectrometer from the ATLAS and EURECA missions, *Solar Physics*, **214**, 1-22, doi:10.1023/A:1024048429145.

Uchiyama A., T. Matsunaga and A. Yamazki, 2017: The instrument constant of sky radiometers (POM-02), Part II; Solid view angle, *Atmos. Meas. Tech.* (to be submitted)

Uchiyama, A., A. Yamazaki, R. Kudo, 2014: Column Water Vapor Retrievals from Sky-radiometer (POM-02) 940nm Data. *J. Meteorol. Soc. Japan*, **92A**, 195-203, DOI:10.2151/jmsj.2014-A13.

Wehrli, C., 1985: Extraterrestrial Solar Spectrum, Publication no. 615, Physikalisch-Meteorologisches Observatorium + World Radiation Center (PMO/WRC) Davos Dorf, Switzerland, July 1985.

Wehrli, C., 2005: GAW–PFR: A network of Aerosol Optical Depth observations with Precision Filter Radiometers. In: WMO/GAW Experts workshop on a global surface based network for long term observations of column aerosol optical properties, Tech. rep., GAW Report No. 162, WMO TD No. 1287, ftp://ftp.wmo.int/Documents/PublicWeb/arep/gaw/gaw162.pdf, 2005.

Yamamoto, Y., Arai, Y., Sakuma, F., 2002: Development of a calibration standard of the spectral radiance for optical sensors, SICE 2002. Proceedings of the 41st SICE

Annual Conference, Vol. 3, 1885–1890, http://dx.doi.org/10.1109/SICE.2002.1196613.

Atmos. Meas. Tech. Discuss., https://doi.org/10.5194/amt-2017-432
Manuscript under review for journal Atmos. Meas. Tech.
Discussion started: 11 January 2018

Atmospheric Measurement Techniques Discussions

Table titles

Table 1 Example of calibration constants (V_0) determined from the data taken at MLO.

Table 2 Results of the calibration constant transferred from POM-02 (Calibration Reference) to POM-02(Tsukuba) and POM-02 (Fukuoka) in December 2014.

Table 3 Statistics of difference between IML method and normal Langley method.

Table 4 Calibration constants for POM-02 determined by using the calibrated integrating sphere measurement

Table 5 Calibration constant at 940 nm by modified Langley method using the data taken at MLO.

Table 6 Same as Table 5 but using the data taken at Tsukuba, MRI.

Figure captions

Fig. 1 Relation between the inside temperature of the instrument and the ambient environmental temperature for POM-02 (Calibration Reference).

Fig. 2 Relation between the sensor output and the inside temperature near the filter turret for POM-02 (Calibration Reference). The sensor output is normalized by that at 20°C. The error bars are the standard deviation. (a) 340, 380, 400, and 500 nm. (b) 675, 870, 940, and 1020 nm. (c) 1225, 1627, and 2200 nm.

Fig. 3 Same as Fig. 2 but for POM-02 (Tsukuba).

Fig. 4 Examples of Langley plots using the data obtained at MLO, on November 3, 2015.

Fig. 5 Annual variation of the calibration constants (V_0) for POM-02 (Calibration Reference).

Fig. 6 Monthly mean values and standard deviation of the inside temperature of POM-02 (Tsukuba) (blue line) and the temperature of the near-infrared detector (red line) from December 2013 to December 2016.

Fig. 7 Monthly means of the temperature correction factors and standard deviation for POM-02 (Tsukuba) from December 2013 to December 2016.

Fig. 8 Time series of the calibration constant for POM-02 (Tsukuba) from January 2014 to December 2015. Blue open squares with error bars denote the calibration constants determined by the IML method. The green line shows the 3-point running mean of IML, and the red line is the calibration constant transferred from POM-02 (Calibration Reference).

Fig. 9 (a) Scatter plot of the optical thickness at 500 nm and V_0 by the IML method for the 500 nm channel. (b) Scatter plot of W_0 and V_0 by the IML method for the 500 nm channel. (c) Time series of V_0 by the IML method for the 500 nm channel from January 2014 to December 2015.

Fig. 10 (a) Extra-terrestrial solar spectra. The red line is Gueymard (2004), the blue line is Thuillier et al. (2003), and the green line is Wehrli (1985). (b) Ratios of the solar spectrum to Gueymard (2003).

Fig. 11 (a) Monthly mean of V_{02}/V_{01} and the standard deviation, here $V_{01} = V_0(500\text{nm})$. (b) Ratio of V_{02} to the interpolated value of the calibration constant determined by the Langley method. The red symbols are 1225 nm, blue ones are 1627 nm, and green ones are 2200 nm.

Atmos. Meas. Tech. Discuss., https://doi.org/10.5194/amt-2017-432
Manuscript under review for journal Atmos. Meas. Tech.
Discussion started: 11 January 2018

Atmospheric Measurement Techniques Discussions
Open Access
EGU

Table 1 Example of calibration constants (V_0) determined from the data taken at MLO.

	Wavelength (nm)	340	380	400	500	675	870	940	1020	1225	1627	2200
Case 1	V0 (NGABS,NTPC)($\times10^{-4}$)	0.19881	0.39320	1.6407	2.7731	3.2849	2.4785	1.9679	1.5521	0.88035	1.4385	0.72407
	SD($\times10^{-4}$)	0.00117	0.00175	0.0062	0.0082	0.0054	0.0145	0.1769	0.0078	0.01116	0.0123	0.00449
	ERR(=SD/V0)	0.00588	0.00446	0.0038	0.0030	0.0016	0.0058	0.0899	0.0050	0.01267	0.0085	0.00621
Case 2	V0 (NGABS,TPC)($\times10^{-4}$)	0.20507	0.39505	1.6470	2.7624	3.2572	2.4820	1.9540	1.5658	0.87322	1.4258	0.68699
	SD($\times10^{-4}$)	0.00179	0.00168	0.0062	0.0078	0.0071	0.0143	0.1759	0.0095	0.01155	0.0132	0.00792
	ERR(=SD/V0)	0.00874	0.00425	0.0038	0.0028	0.0022	0.0058	0.0900	0.0061	0.01323	0.0093	0.01153
Case 3	V0 (GABS,NTPC) ($\times10^{-4}$)	0.19881	0.39319	1.6407	2.7732	3.2850	2.4785	2.3426	1.5524	0.88353	1.4397	0.73073
	SD($\times10^{-4}$)	0.00117	0.00175	0.0062	0.0081	0.0054	0.0144	0.2356	0.0078	0.01080	0.0122	0.00442
	ERR(=SD/V0)	0.00588	0.00445	0.0038	0.0029	0.0016	0.0058	0.1006	0.0050	0.01222	0.0085	0.00604
Case 4	V0 (GABS,TPC) ($\times10^{-4}$)	0.20506	0.39504	1.6469	2.7626	3.2573	2.4820	2.3261	1.5664	0.87646	1.4268	0.69471
	SD($\times10^{-4}$)	0.00179	0.00168	0.0062	0.0078	0.0072	0.0143	0.2340	0.0098	0.01133	0.0132	0.00837
	ERR(=SD/V0)	0.00874	0.00425	0.0038	0.0028	0.0022	0.0057	0.1006	0.0062	0.01292	0.0093	0.01205
	(Case 1)/(Case 4) − 1.0	−0.0305	−0.0047	−0.0038	0.0038	0.0085	−0.0014	−0.1540	−0.0091	0.0044	0.0082	0.0423
	(Case 2)/(Case 4) − 1.0	0.0000	0.0000	0.0001	−0.0001	0.0000	0.0000	−0.1600	−0.0004	−0.0037	−0.0007	−0.0111
	(Case 3)/(Case 4) − 1.0	−0.0305	−0.0047	−0.0038	0.0038	0.0085	−0.0014	0.0071	−0.0089	0.0081	0.0090	0.0518

(dark shading) : ABS(ERR)> 0.03 (light shading) : ABS(ERR)<0.01

V0: mean value of calibration constant in 2015 MLO observation

SD: standard deviation

ERR=SD/V0

GABS: consideration of gas absorption

NGABS: no consideration of gas absorption

Atmos. Meas. Tech. Discuss., https://doi.org/10.5194/amt-2017-432
Manuscript under review for journal Atmos. Meas. Tech.
Discussion started: 11 January 2018

Atmospheric Measurement Techniques Discussions

TPC: consideration of temperature correction

NTPC: no consideration of temperature correction

Table 2 Results of the calibration constant transferred from POM-02 (Calibration Reference) to POM-02(Tsukuba) and POM-02 (Fukuoka) in December 2014.

Site: Tsukuba

Period 2015/12/01 to 2016/01/01

No. of days 11

SN PS1202091 Calibrated by Sky radiometer PS1207831

Wavelength (nm)	340	380	400	500	675	870	940	1020	1225	1627	2200
V_0 (×10⁻⁴)	0.17469	0.25711	1.1621	2.9248	3.4792	2.2969	1.9900	0.79227	0.87065	1.4074	0.76879
SD (×10⁻⁴)	0.00050	0.00065	0.0021	0.0039	0.0045	0.0085	0.0087	0.00427	0.00321	0.0072	0.00402
ERR (=SD/V0)	0.00284	0.00253	0.0018	0.0013	0.0013	0.0037	0.0044	0.00539	0.00369	0.0051	0.00523

Site: Fukuoka

Period 2015/12/4 to 2015/12/20

No. of days 8

SN PS1202071 Calibrated by Skyradiometer PS1207831

Wavelength (nm)	340	380	400	500	675	870	940	1020	1225	1627	2200
V_0 (×10⁻⁴)	0.18374	0.23346	1.2332	2.9179	3.5176	2.3021	1.9827	1.8899	0.84113	1.2783	0.60461
SD (×10⁻⁴)	0.00028	0.00025	0.0014	0.0025	0.0041	0.0044	0.0106	0.0031	0.00279	0.0027	0.00113
ERR (=SD/V0)	0.00155	0.00107	0.0011	0.0008	0.0012	0.0019	0.0053	0.0016	0.00331	0.0021	0.00186

V0 : mean value,

SD: standard deviation

Atmos. Meas. Tech. Discuss., https://doi.org/10.5194/amt-2017-432
Manuscript under review for journal Atmos. Meas. Tech.
Discussion started: 11 January 2018

Atmospheric Measurement Techniques
Discussions

Table 3 Statistics of difference between IML method and normal Langley method.

Wavelength (nm)	340	380	400	500	675	870	1020
V0 (×10⁻⁴)	0.17600	0.26022	1.1840	2.9161	3.4681	2.2863	1.2487
BIAS (×10⁻⁴)	−0.00136	−0.00428	−0.0042	0.0083	−0.0125	0.0017	0.0048
RMS (×10⁻⁴)	0.00325	0.00649	0.0198	0.0225	0.0209	0.0197	0.0309
DFMAX (×10⁻⁴)	0.00725	0.01218	0.0368	0.0475	0.0445	0.0489	0.0558
DFMIN (×10⁻⁴)	0.00006	0.00059	0.0004	0.0011	0.0028	0.0002	0.0006
BIAS/V0	−0.0077	−0.0164	−0.0036	0.0028	−0.0036	0.0008	0.0039
RMS/V0	0.0184	0.0249	0.0167	0.0077	0.0060	0.0086	0.0247
DFMAX/V0	0.0412	0.0468	0.0311	0.0163	0.0128	0.0214	0.0447
DFMIN/V0	0.0003	0.0023	0.0004	0.0004	0.0008	0.0001	0.0005
V0_3RM (×10⁻⁴)	0.17604	0.26037	1.1848	2.9150	3.4678	2.2858	1.2794
BIAS (×10⁻⁴)	−0.00114	−0.00389	−0.0030	0.0093	−0.0124	0.0022	0.0030
RMS (×10⁻⁴)	0.00303	0.00594	0.0178	0.0181	0.0171	0.0163	0.1014
DFMAX (×10⁻⁴)	0.00495	0.01065	0.0321	0.0398	0.0352	0.0338	0.3663
DFMIN (×10⁻⁴)	0.00022	0.00006	0.0007	0.0032	0.0013	0.0006	0.0004
BIAS/ V0_3RM	−0.0065	−0.0149	−0.0025	0.0032	−0.0036	0.0010	0.0023
RMS/ V0_3RM	0.0172	0.0228	0.0150	0.0062	0.0049	0.0071	0.0793
DFMAX/ V0_3RM	0.0281	0.0409	0.0271	0.0137	0.0102	0.0148	0.2863
DFMIN/ V0_3RM	0.0013	0.0002	0.0006	0.0011	0.0004	0.0002	0.0003

V0: mean calibration constant (IML method) during Jan. 2014 to Dec. 2015.

V0_3RM: mean calibration constant (IML method, 3-point running mean) during Jan. 2014 to Dec. 2015.

BIAS: bias (mean of differences between IML and normal Langley methods)

RMS: root mean squares of differences between IML and normal Langley methods

DFMAX: maximum difference between IML and normal Langley methods

Atmos. Meas. Tech. Discuss., https://doi.org/10.5194/amt-2017-432
Manuscript under review for journal Atmos. Meas. Tech.
Discussion started: 11 January 2018

Atmospheric Measurement Techniques Discussions

DFMIN: minimum difference between IML and normal Langley methods

Table 4 Calibration constants for POM-02 determined by using the calibrated integrating sphere measurement

λ_0 (nm)	$\bar{F}_0$ (mW/m²/nm)	$\bar{I}_{sph}$ (mW/m²/sr/nm)	$\Delta\Omega$ (×10⁻⁴) (sr)	V_{sph} (×10⁻¹⁰)	V_{sun} (×10⁻⁴)	V_0 (×10⁻⁴)	$(V_{sun} - V_0)/V_0$ (%)	I
340	1036.2	-	2.3970	-	-	0.19884	-	-
380	1210.6	24.5	2.4370	1.9699	0.39941	0.39280	1.68	PTFE(4.17A(50W)x4)
400	1523.3	49.6	2.4190	13.376	1.6982	1.6434	3.34	PTFE(4.17A(50W)x4)
500	1964.6	238.1	2.4170	87.342	2.9817	2.7703	7.63	PTFE(4.17A(50W)x4)
675	1496.5	764.1	2.4220	409.02	3.3075	3.2850	0.69	PTFE(4.17A(50W)x4)
870	958.1	1171.1	2.4310	772.57	2.6000	2.4708	5.23	PTFE(4.17A(50W)x4)
940	822.0	1218.8	2.4520	878.84	2.4173	2.3364	3.46	PTFE(4.17A(50W)x4)
1020	698.1	1236.8	2.4520	682.48	1.5710	1.5559	0.97	PTFE(4.17A(50W)x4)
1225	466.5	537.3	1.9800	204.73	0.89767	0.88715	1.19	PTFE(3.30A(50W)x4)
1627	236.0	377.2	2.0000	459.62	1.4378	1.4456	-0.54	PTFE(3.30A(50W)x4)
2200	82.0	128.2	2.0570	237.19	0.73756	0.72472	1.77	PTFE(3.30A(50W)x4)

V_0: calibration constant by normal Langley method

Atmos. Meas. Tech. Discuss., https://doi.org/10.5194/amt-2017-432
Manuscript under review for journal Atmos. Meas. Tech.
Discussion started: 11 January 2018

Table 5 Calibration constant at 940 nm by modified Langley method using the data taken at MLO.

		Langley	modified Langley	Ratio
2014	V0 ($\times 10^{-4}$)	2.3364	2.2973	0.9833
	SD ($\times 10^{-4}$)	0.2183	0.1195	
	SD/V0	0.0934	0.0520	
	No. of data	19	19	
2015	V0 ($\times 10^{-4}$)	2.3157	2.2954	0.9912
	SD ($\times 10^{-4}$)	0.2236	0.1077	
	SD/V0	0.0966	0.0469	
	No. of data	30	20	

The data taken at MLO in 2014 and 2015 were used.
V0: mean value
SD: standard deviation
Ratio = (modified Langley V0)/(Langley V0)

Atmos. Meas. Tech. Discuss., https://doi.org/10.5194/amt-2017-432
Manuscript under review for journal Atmos. Meas. Tech.
Discussion started: 11 January 2018

Atmospheric Measurement Techniques
Discussions

Table 6 Same as Table 5 but using the data taken at Tsukuba, MRI.

		Langley	modified Langley	Ratio
2014	V0 ($\times 10^{-4}$)	2.3343	2.3562	1.0094
	SD ($\times 10^{-4}$)	0.0002	0.1429	
	SD/V0	0.0001	0.0598	
	No. of data	10	10	
2015	V0 ($\times 10^{-4}$)	2.3132	2.3090	0.9982
	SD ($\times 10^{-4}$)	0.0006	0.1043	
	SD/V0	0.0003	0.0452	
	No. of data	17	17	

The data taken at MRI, Tsukuba in December 2014 and December 2015 were used.

V0: mean value

SD: standard deviation

Ratio = (modified Langley V0)/(Langley V0)

Atmos. Meas. Tech. Discuss., https://doi.org/10.5194/amt-2017-432
Manuscript under review for journal Atmos. Meas. Tech.
Discussion started: 11 January 2018

Atmospheric Measurement Techniques
Discussions

Fig.1

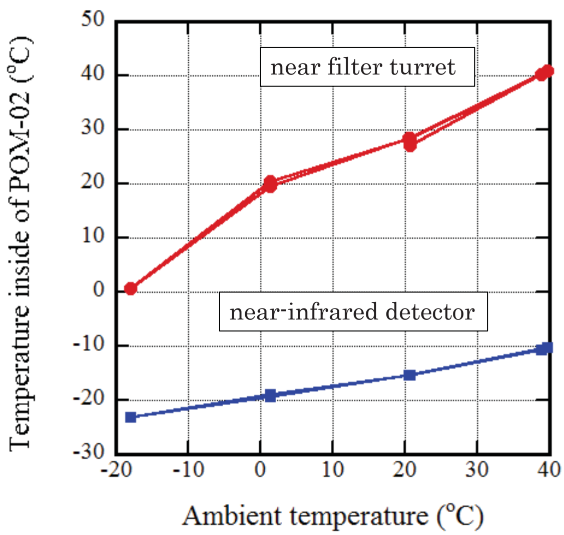

Fig. 1 Relation between the inside temperature of instrument and the ambient environmental one for POM-02 (Calibration Reference).

Fig. 2

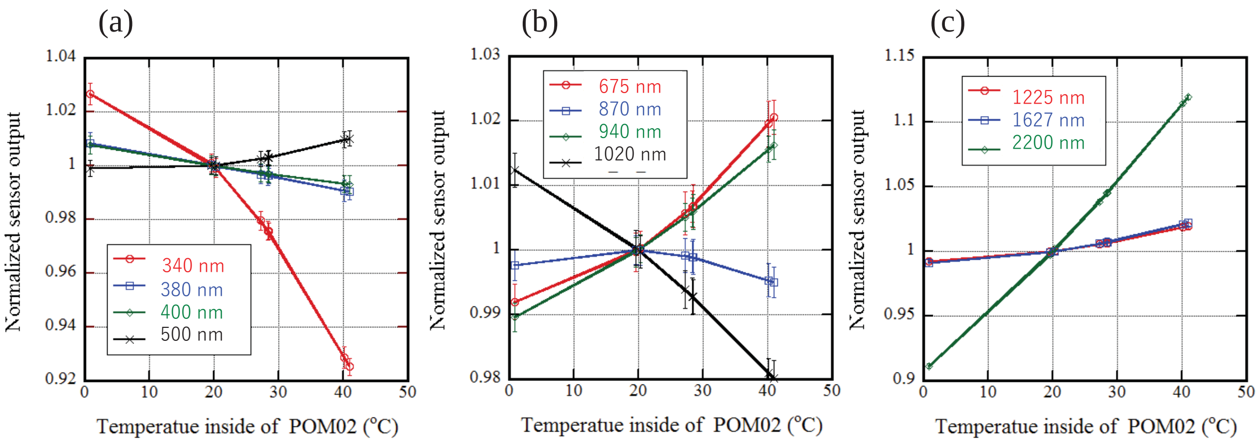

Fig. 2 Relation between sensor output and the inside temperature near filter turret for POM-02 (Calibration Reference). The sensor output is normalized by that at 20° C, (a) 340, 380, 400 and 500nm. (b) 675, 870, 940 and 1020nm. (a)1225, 1627 and 2200nm.

Fig. 3

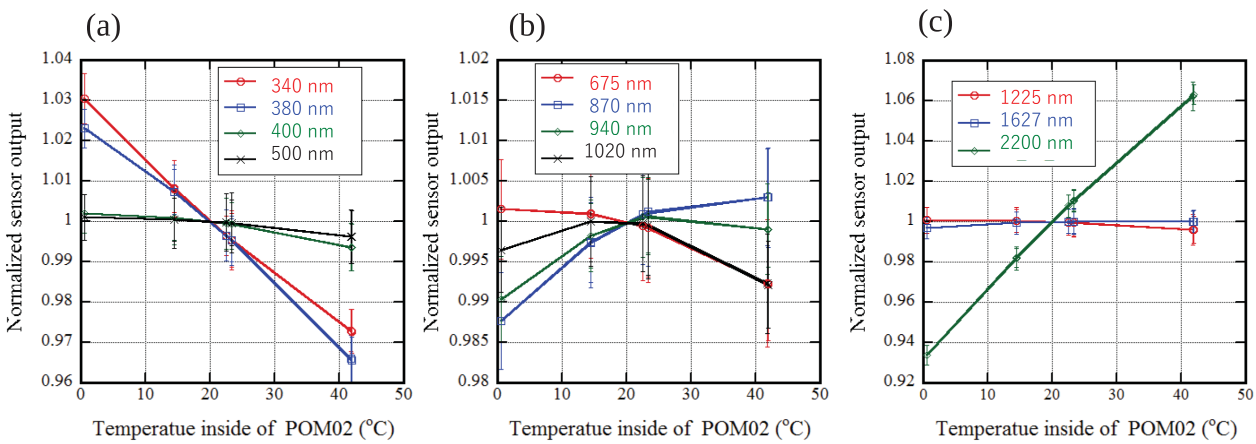

Fig. 3 Same as Fig. 2 but for POM-02 (Tsukuba).

Atmos. Meas. Tech. Discuss., https://doi.org/10.5194/amt-2017-432
Manuscript under review for journal Atmos. Meas. Tech.
Discussion started: 11 January 2018

Fig. 4

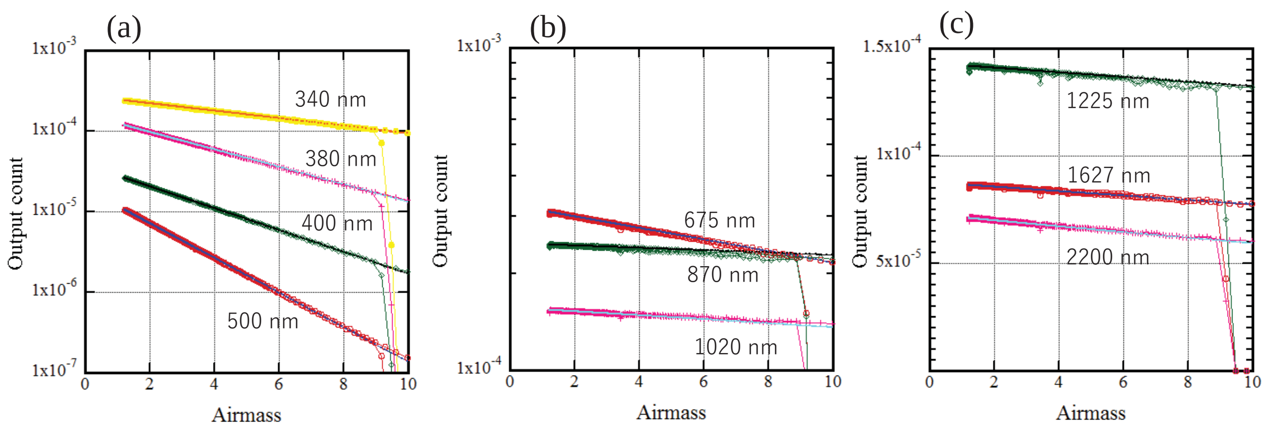

Fig. 4 Examples of Langley plots using the data obtained at MLO, on November 3, 2015.

Atmos. Meas. Tech. Discuss., https://doi.org/10.5194/amt-2017-432
Manuscript under review for journal Atmos. Meas. Tech.
Discussion started: 11 January 2018

Atmospheric Measurement Techniques
Open Access
Discussions

Fig. 5

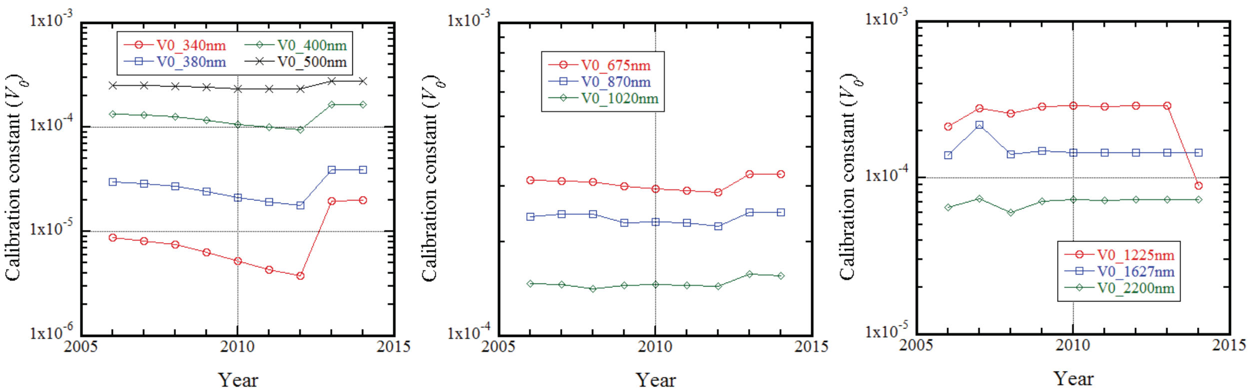

Fig. 5 The annual variation of the calibration constants (V_0) for POM-02 (Calibration Reference).

Atmos. Meas. Tech. Discuss., https://doi.org/10.5194/amt-2017-432
Manuscript under review for journal Atmos. Meas. Tech.
Discussion started: 11 January 2018

Atmospheric Measurement Techniques
Discussions

Fig. 6

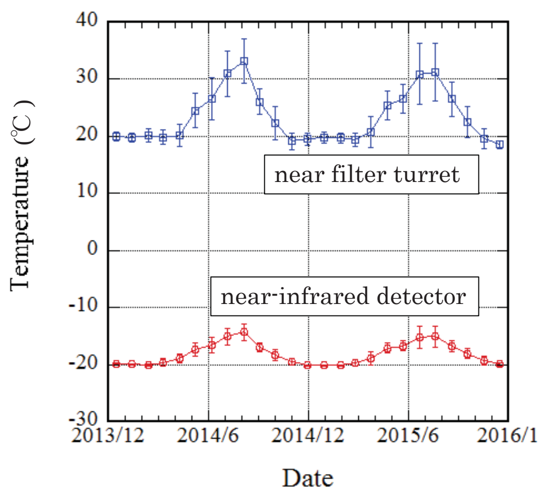

Fig. 6 Monthly mean values and standard deviation of the inside temperature of POM-02 (Tsukuba) (blue line) and the temperature of near-infrared detector (red line) from December, 2013 to December, 2016.

Fig. 7

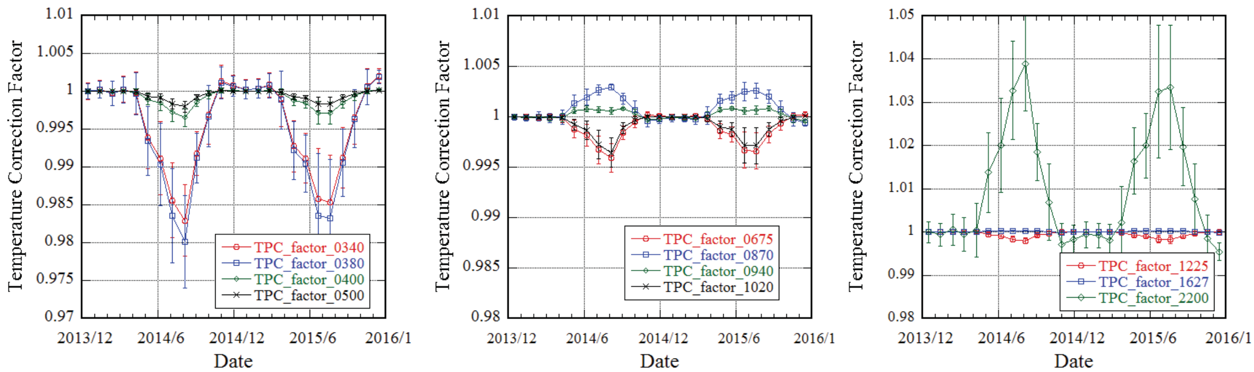

Fig. 7 The monthly means of temperature correction factors and standard deviation for POM-02 (Tsukuba) from December, 2013 to December, 2016.

Atmos. Meas. Tech. Discuss., https://doi.org/10.5194/amt-2017-432
Manuscript under review for journal Atmos. Meas. Tech.
Discussion started: 11 January 2018

Atmospheric Measurement Techniques
Discussions

Fig. 8

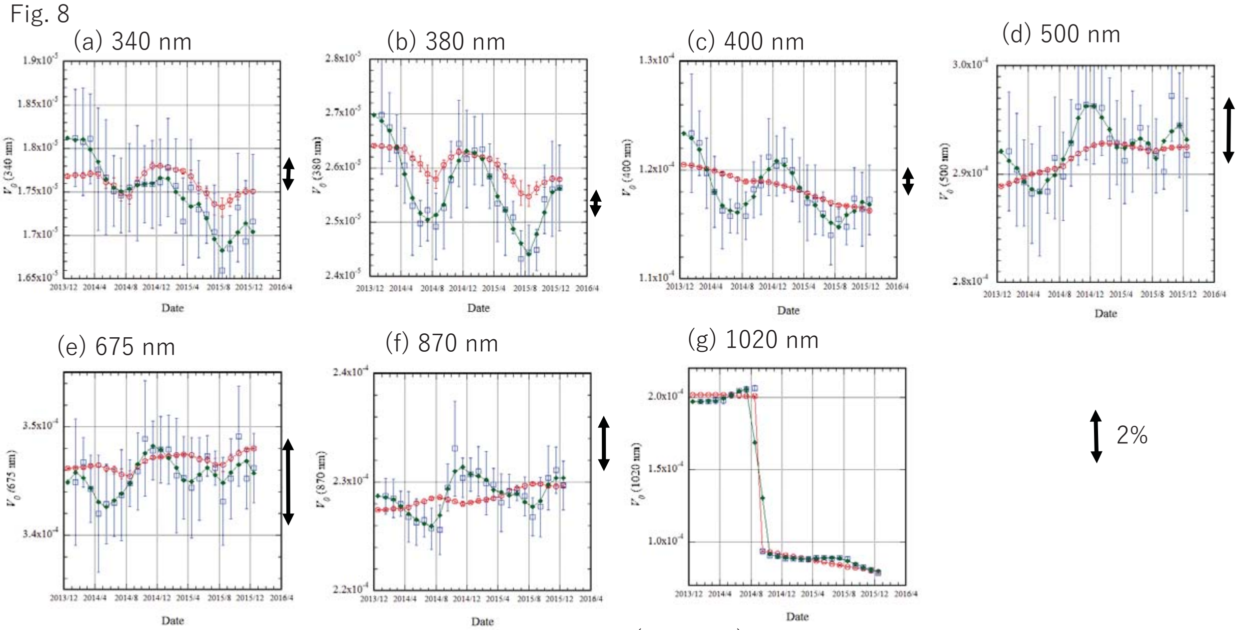

Fig. 8 Time series of calibration constant for POM-02 (Tsukuba) from January, 2014 to December, 2015. Blue open squares with error bar is calibration constant determined by IML method, Green line is 3 points running mean of IML, and Red line is calibration constant transferred from POM-02 (Calibration Reference).

Atmos. Meas. Tech. Discuss., https://doi.org/10.5194/amt-2017-432
Manuscript under review for journal Atmos. Meas. Tech.
Discussion started: 11 January 2018

Fig. 9

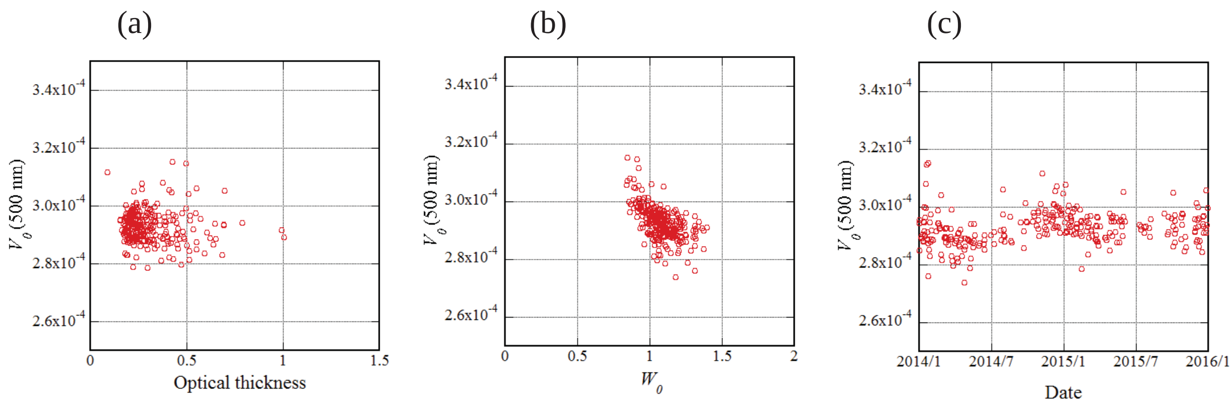

Fig. 9 (a) scatter plot of optical thickness at 500nm and V_0 by the IML method for 500nm channel, (b) scatter plot of W_0 and V_0 by the IML method for 500nm channel, (c) time series of V_0 by the IML method for 500nm channel in the period from January 2014 to December 2015 are shown.

Atmos. Meas. Tech. Discuss., https://doi.org/10.5194/amt-2017-432
Manuscript under review for journal Atmos. Meas. Tech.
Discussion started: 11 January 2018

Atmospheric Measurement Techniques Discussions
Open Access

Fig. 10

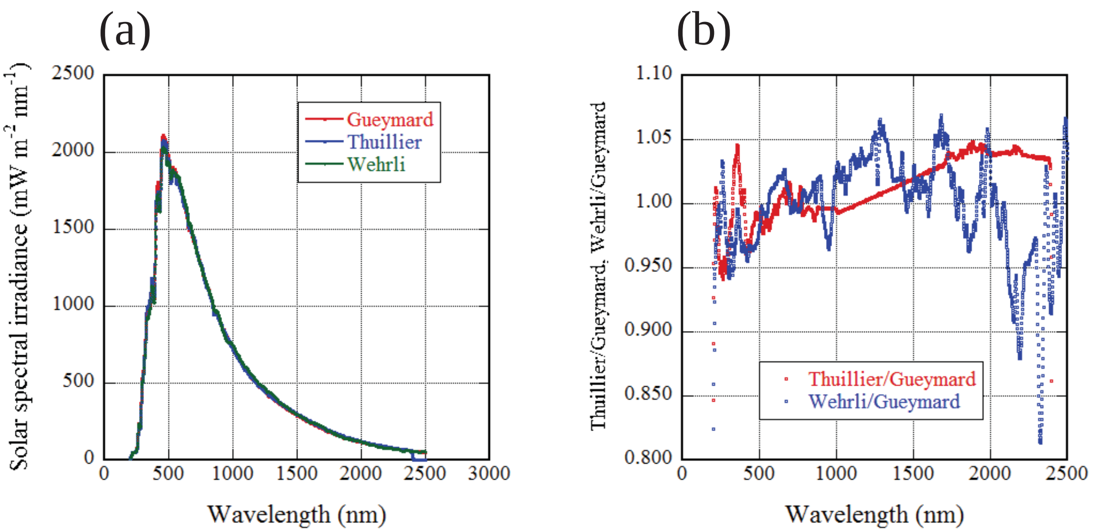

Fig. 10 (a) extra-terrestrial solar spectra, red line is Gueymard (2003), blue line is Thuillier et al (2003), and green line is Wehrli (1985), (b) the ratios of the solar spectrum to Gueymard (2003).

Atmos. Meas. Tech. Discuss., https://doi.org/10.5194/amt-2017-432
Manuscript under review for journal Atmos. Meas. Tech.
Discussion started: 11 January 2018

Fig. 11

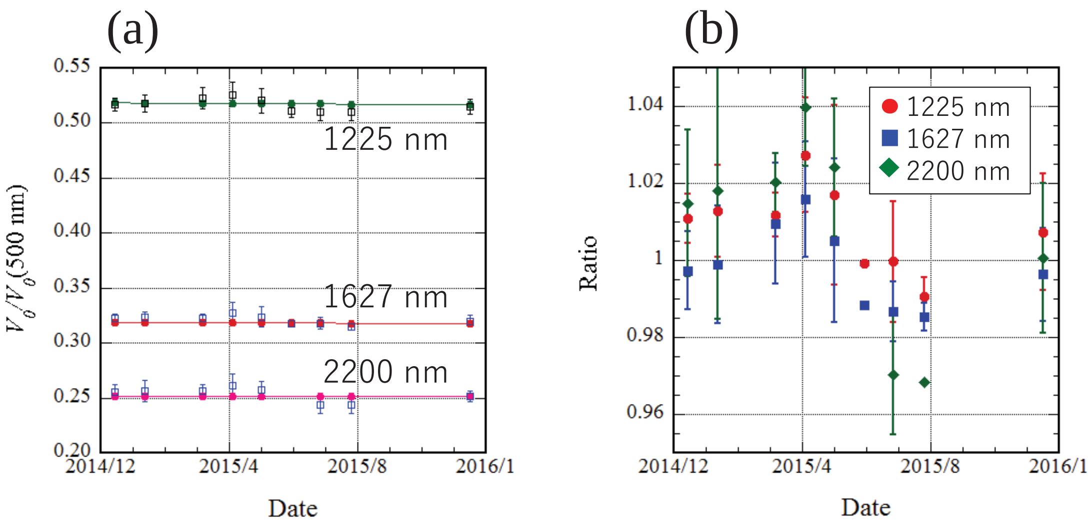

Fig. 11 (a) monthly mean of V_{02}/V_{01} and standard deviation, here $V_{01}=V_0$(500 nm), (b) Ratio of V_{02} to the interpolated value of the calibration constant determined by Langley method, red symbols are 1225nm, blue ones are 1627nm, and green ones are 2200nm